



Since January 2020 Elsevier has created a COVID-19 resource centre with free information in English and Mandarin on the novel coronavirus COVID-19. The COVID-19 resource centre is hosted on Elsevier Connect, the company's public news and information website.

Elsevier hereby grants permission to make all its COVID-19-related research that is available on the COVID-19 resource centre - including this research content - immediately available in PubMed Central and other publicly funded repositories, such as the WHO COVID database with rights for unrestricted research re-use and analyses in any form or by any means with acknowledgement of the original source. These permissions are granted for free by Elsevier for as long as the COVID-19 resource centre remains active.



# Dual challenges of heat wave and protective facemask-induced thermal stress in Hong Kong

Dachuan Shi<sup>a</sup>, Jiyun Song<sup>a,b,\*</sup>, Ruiqing Du<sup>a</sup>, Pak Wai Chan<sup>c</sup>

<sup>a</sup> Department of Mechanical Engineering, The University of Hong Kong, Pokfulam Road, Hong Kong SAR, China

<sup>b</sup> Department of Geography, The University of Hong Kong, Pokfulam Road, Hong Kong SAR, China

<sup>c</sup> Hong Kong Observatory, Hong Kong SAR, China

## ARTICLE INFO

### Keywords:

Protective facemask  
Human thermal stress  
Physiological subjective temperature  
Heat wave  
Microclimate  
Topography

## ABSTRACT

During the COVID-19 pandemic, wearing protective facemasks (PFMs) can effectively reduce infection risk, but the use of PFMs can amplify heat-related health risks. We studied the amplified PFM-induced human thermal stress via both field measurements and model simulations over a typical subtropical mountainous city, Hong Kong. First, a hot and humid PFM microenvironment has been observed with high temperature (34–35 °C) and high humidity (80–95%), resulting in an aggravated facial thermal stress with a maximal PFM-covered facial heat flux of 500 W/m<sup>2</sup> under high-intensity activities. Second, to predict the overall PFM-inclusive human thermal stress, we developed a new facial thermal load model,  $S_{PFM}$  and a new human-environment adaptive thermal stress (HEATS) model by coupling  $S_{PFM}$  with an enhanced thermal comfort model to resolve modified human-environment interactions with the intervention of PFM under realistic climatic and topographical conditions. The model was then applied to predict spatiotemporal variations of PFM-inclusive physiological subjective temperature (PST) and corresponding heat stress levels during a typical heat wave event. It was found wearing PFM can significantly aggravate human thermal stress over Hong Kong with a spatially averaged PST increment of 5.0 °C and an additional spatial area of 158.4% exposed to the severest heat risks. Besides, PFM-inclusive PST was found to increase nonlinearly with terrain slopes at a rate of 1.3–3.9 °C/10°(slope), owing to elevated metabolic heat production. Furthermore, urban residents were found to have higher PFM-aggravated heat risks than rural residents, especially at night due to synergistic urban heat and moisture island effects.

## 1. Introduction

Recent decades have seen hotter summers with more frequent extreme heat events worldwide due to global warming and excessive anthropogenic emissions, with a consequence of more heat-related mortality and morbidity. Future climate projection studies have shown that the frequency, intensity, and duration of global heat waves are expected to increase considerably, resulting in a greater impact on population health [1,2]. The ongoing COVID-19 pandemic has put the world population into a more dangerous context with dual challenges of infection and heat stress [3], especially for people in densely populated Northeast India and West Africa where are with limited cooling infrastructure and poor public health facilities. Wearing protective facemasks (PFMs) has been proven to be one of the most effective interventions to reduce the infection risk. However, the use of PFMs can amplify heat-related health risks due to impeded heat dissipation through

convective and respiratory exchanges. This could be a serious problem for the public, especially in vulnerable populations including people with COVID-19 sequelae, people with respiratory and cardiovascular diseases, outdoor workers, health workers, athletes, pregnant women, the poor, children, and the elderly [4].

Although the PFM-covered facial area is very small compared to the human body surface area, its impact on human thermoregulation and thermal sensation is critical [5]. Firstly, due to very high metabolic activity levels in the human head, the heat flux of bare facial skin area (104 W/m<sup>2</sup>) is more than twice that of the remaining body surface area (50 W/m<sup>2</sup>) [6]. The use of PFMs can significantly impede facial heat dissipation via respiration, convection, radiation, and evaporation, resulting in an elevated facial skin temperature. Secondly, the facial area covered by PFMs is very thermosensitive containing a high density of thermoreceptors, thus the elevated facial skin temperature and aggravated hot humid PFM microenvironment will significantly influence

\* Corresponding author. Department of Mechanical Engineering, The University of Hong Kong, Pokfulam Road, Hong Kong SAR, China.  
E-mail address: [jsong90@hku.hk](mailto:jsong90@hku.hk) (J. Song).

<https://doi.org/10.1016/j.buildenv.2021.108317>

Received 15 May 2021; Received in revised form 24 August 2021; Accepted 28 August 2021

Available online 1 September 2021

0360-1323/© 2021 Elsevier Ltd. All rights reserved.

human thermal sensations [7]. Previous PFM-related thermal studies mainly focused on investigating PFM-induced facial thermal sensations via field experiments and questionnaires with volunteers standing/sitting indoor under a steady state [8–11], the quantification of PFM-induced facial thermal load and PFM-inclusive human thermoregulation under different outdoor activities and climatic conditions is still lack of exploration.

In this study, we aim to fill in the gap and conduct a comprehensive investigation on how PFMs will affect human thermoregulation in people's daily life under different activity levels and different climatic conditions. More specifically, we will (1) develop a new PFM microenvironment model by considering the facial skin energy balance, (2) develop a new PFM-inclusive human thermal comfort model by dynamically coupling the new PFM microenvironment model with an advanced human thermoregulation model. To achieve these research objectives, an appropriate human thermal comfort model needs to be first selected. Classical thermal comfort models can be divided into three main categories, including one-node model, two-node model, and multi-node model. One-node models (e.g., Fanger's PMV model [12], Jendritzky's advanced PMV model [13], Błażejczyk's MENEX model [14]), are used to quantify the average adaptive steady-state thermal comfort condition of a whole human body by resolving human-environment interactions. On the other hand, two-node models (e.g., Gagge's model [15], Kaynakli and Kilic [16], Foda and Sirén [17], etc.) and multi-node models (e.g., Fiala model [18], Tanabe model [19] and UCB model [20], etc.) are used to quantify more detailed transient thermal comfort conditions of different human body segments by considering a two-layer structure (skin and core) [21] and a multi-segment structure (skin, fat, muscle, bone, etc.), respectively. Here, the one-node MENEX model [14] with high predictive accuracy and small computational cost is selected as the basic framework for further development of our new PFM-inclusive human thermal comfort model, which will be applied in both local and city scales.

The newly proposed methodology will be tested over a stereotyped high-rise compact hot and humid metropolitan area, Hong Kong, where over 95% of people wear PFMs outdoor, for case study. Hong Kong is known for its hot-humid summers with afternoon temperature often exceeding 31° and nighttime temperature remaining around 26 °C with high humidity, based on past 30 years' meteorological records (1991–2020) [22]. High temperature and high humidity restrain the human body's cooling efficiency via thermal radiation and sweat evaporation, respectively, thus leading to severe human thermal stresses [23–25]. On the other hand, it is noteworthy that Hong Kong is featured with rugged terrains with slope ranging from 0° to 77° [26], which implies that residents may face greater heat risks from elevated metabolic heat production and expenditure when climbing over inclined terrains compared to walking over flat terrains [27].

Thus, it is of urgent need to quantify the aggravated human thermal stress due to PFM wearing over Hong Kong, so that timely actions can be taken by the government and public. Particularly, it is important to know how PFM aggravates human thermal stress under different activity levels and which neighbourhoods are most vulnerable to PFM-inclusive heat stress. To address these questions, we conducted a comprehensive investigation on PFM-induced facial thermal stress and PFM-inclusive human thermal stress via field experiments and numerical model simulations, respectively. In the field experimental phase, we observed and compared different thermo-physiological responses of subjects with and without PFMs at different activities (standing, walking, and climbing). In the numerical model simulation phase, we developed a new PFM-inclusive human-environment adaptive thermal stress (HEATS) model with the consideration of PFM-modified human thermoregulation schemes under realistic climatic and topographical conditions. The newly proposed PFM-inclusive HEATS model is featured with the following advanced characteristics, including the consideration of the intervention of facemasks in heat dissipation and the implication of city topography on human metabolism and energy expenditure. With the

HEATS model, we predicted a PFM-inclusive heat stress map during a typical heat wave event over the Hong Kong metropolitan area, which can provide neighbourhood-scale heat risk warnings so that the public can be better prepared in their daily life under the dual challenges of pandemic and heat risks.

## 2. Methodology

### 2.1. A new human-environment adaptive thermal stress model

In this section, we propose a new human-environment adaptive thermal stress (HEATS) model with the capability of considering PFM-modified human thermoregulation schemes under realistic climatic and topographical conditions (Fig. 1). The governing equation of the new HEATS model is human energy balance [28]:

$$S = M + R_{nh} - W - (C + E)_{body} - (C + E)_{res}, \quad (1)$$

where  $S$  is the net heat storage,  $M$  is the metabolic heat production,  $R_{nh}$  is the net radiation of the human body (which considers the absorption and reflection of shortwave and longwave radiation between human body and the environment),  $W$  is the mechanical work,  $C$  and  $E$  is the heat dissipation via convection and evaporation, respectively, with the subscripts of "body" and "res" indicating from body surface and respiration, respectively. All terms are expressed in  $W/m^2$ . It is noteworthy that classic PFM-exclusive human energy balance can be referred to the MENEX model [14,28], for instance, the calculation procedure of the heat dissipation via human body surfaces, i.e.,  $(C + E)_{body}$  is cited and shown in Appendix 1 [29]. In the following two sub-sections, we focus on introducing two newly proposed modules, i.e.,  $S_{PFM}$ -HEATS and  $Top$ -HEATS, by considering the extra heat burden in the human energy balance equation (Eqn. (1)) due to the wearing of PFM and topography-induced human activity levels, respectively.

#### 2.1.1. $S_{PFM}$ -HEATS module

First, the usage of PFM can suppress facial heat dissipation via convection, evaporation, radiation, conduction, and respiration. To quantify the PFM-induced facial thermal load, we developed a  $S_{PFM}$  model (see Fig. 1b) based on skin energy balance. As shown in Fig. 1b, the PFM surface was regarded as the upper boundary of the PFM microenvironment, while the face surface was regarded as the lower boundary.  $S_{PFM}$  is the PFM-induced facial thermal load due to suppressed facial heat dissipation,

$$S_{PFM} = (C + E + R)_{fsk} + G_{pfm} + (C + E)_{res} - Q, \quad (2)$$

where  $C$ ,  $E$ ,  $R$ ,  $G$  denote convection, evaporation, radiation, and conduction, respectively, with the subscripts "fsk" and "res" representing for facial skin and respiration, respectively.  $(C + E + R)_{fsk}$  can be calculated according to general skin energy balance equations [14].  $G_{pfm}$  can be calculated according to PFM surface energy balance equation ( $G_{pfm} = R_n - H - LE$ ), where  $R_n$  is the net radiation received by the PFM,  $H$  is the PFM surface sensible heat flux calculated via  $H_{pfm} = (1 - a_{pfm}) \rho c_p (T_{sk} - T_a)$ , and  $LE$  is the PFM surface latent heat flux. In current default settings,  $LE = 0$ ; in special settings if the PFM is wet or the PFM is made from phase change materials,  $LE \neq 0$ .  $Q$  is the convective heat exchange between PFM cavity and ambient air due to leakage.  $(C + E)_{res}$  is the suppressed heat dissipation from respiration [28]:

$$(C + E)_{res} = 0.0014 \cdot M \cdot (34 - T_{in}) + 0.0173 \cdot M \cdot (5.87 - p_{in}), \quad (3)$$

where  $T_{in}$  and  $p_{in}$  denote air temperature and pressure inside the PFM, respectively.

Then, the modified governing equation of coupled  $S_{PFM}$ -HEATS model is:

$$S = M + R_{nh} - (C + E)_{body} + S_{PFM}. \quad (4)$$

Detailed information about each variable in the  $S_{PFM}$  model is shown

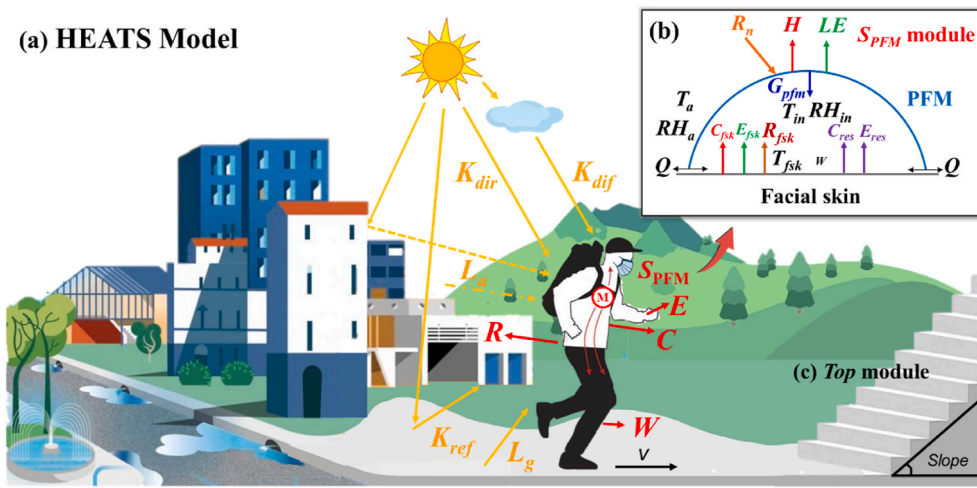


Fig. 1. Sketch of the proposed (a) HEATS model, (b) PFM-induced facial thermal load module ( $S_{PFM}$ ), and (c) topography-induced thermal stress module ( $Top$ ). Figure elements are adopted and reformed from website sources [30–32].

in Table 1.

### 2.2. Top-HEATS module

Second, due to the spatial variability of terrain gradients (Fig. 1c), people tend to move at different walking speed ( $v$ ), metabolic rate ( $M$ ), and mechanical work ( $W$ ). To better capture the topography-induced thermal stress, we developed a *Top*-HEATS module equipped with more realistic equations for  $v$ ,  $M$ , and  $W$  considering the impact of terrain gradients (Fig. 1c). The walking speed ( $v$ , m/s) can be determined by Irmischer-Clarke’s modified version of the Tobler hiking function [33,34]:

$$v = 0.11 + e^{\frac{(-100 \cdot \tan(\text{slope})) + 51^2}{2 \times 30^2}}, \quad (5)$$

where *slope* is the terrain gradient (deg °).

On the other hand, metabolic rate ( $M$ ) is usually crudely assumed via the conventional ISO method based on typical activity classes, including resting (Level 0: 55–70 W/m<sup>2</sup>), low metabolic rate (Level 1: 70–130 W/m<sup>2</sup>), moderate metabolic rate (Level 2: 130–200 W/m<sup>2</sup>), high metabolic

rate (Level 3: 200–260 W/m<sup>2</sup>), and very high metabolic rate (Level 4: >260 W/m<sup>2</sup>) according to BS EN ISO 8996:2004 [35], which cannot represent the spatiotemporal variation of  $M$  due to different terrain gradients and walking speeds. To overcome these limitations in the conventional ISO method, we adopt Looney’s modified version of Pandolf’s predictive equation (Eqn. (6)), which was derived from steady-state exercise protocols (the derivation of Pandolf’s predictive equation is detailed in Appendix 2) [33,36]:

$$M = 1.5 \cdot m + 2.0 \cdot (m + l)(l/m)^2 + \eta \cdot (m + l) \cdot (1.5 \cdot v^2 + 0.35 \cdot v \cdot \text{slope}), \quad (6)$$

where  $m$  is the average human body weight, kg ( $m = 60$  kg in this study),  $l$  is the carriage loads, kg,  $\eta$  is terrain coefficient (1.0 for hard surfaces or pavements).

In addition, to better represent the spatiotemporal variation of  $W$ , we determine mechanical work ( $W$ , W/m<sup>2</sup>) based on realistic walking speeds and terrain gradients [28], as

$$W = m \cdot g \cdot v \cdot \sin(\text{slope}) / A, \quad (7)$$

where  $g$  is the acceleration rate due to gravity (m/s<sup>2</sup>),  $A$  is a standard value of body surface area ( $A = 1.8$  m<sup>2</sup> in this study [28]).

Then, the modified governing equation of coupled *Top*-HEATS model is:

$$S = M + R_{nh} - W - (C + E)_{body} - (C + E)_{res}. \quad (8)$$

Overall, the proposed HEATS model in this section is a new thermal comfort model built upon a basic MENEX model framework of human energy balance [29] and enhanced by adding two new modules,  $S_{PFM}$ -HEATS and *Top*-HEATS, featuring with the capability of predicting human thermal stress due to the wearing of PFMs and the impact of city topography. To drive the HEATS model, meteorological parameters, terrain data, physiological parameters, clothing properties, and PFM thermal characteristics need to be collected as inputs (Table 2). With the HEATS model, we can calculate Physiological Subjective Temperature (PST), i.e., the level of thermal stimuli of a pedestrian after 15–20 min of adaptation to the ambient environment based on the net heat storage  $S$  of the body and inner mean radiant temperature under clothing [14,37, 38]. According to the PST values, we can further assess thermal stress levels according to PST, i.e., level 0 – comfortable (14.1–24 °C), level 1 – warm (24.1–34 °C), level 2 – hot (34.1–44 °C), level 3 – very hot (44.1–54 °C), and level 4 – sweltering (>54 °C).

Table 1  
Variables in the PFM-induced facial thermal load model ( $S_{PFM}$ ).

	Symbol	Unit	Source
<b>Outside the PFM</b>			
● Ambient air temperature	$T_a$	°C	Measured
● Ambient relative humidity	$RH_a$	%	Measured
● Density of air	$\rho$	kg/m <sup>3</sup>	Measured
● Heat capacity of air	$c_p$	kg·m <sup>-2</sup> ·s <sup>-2</sup> ·K <sup>-1</sup>	Measured
● Sensible heat flux	$H$	W/m <sup>2</sup>	Calculated
● Net radiation	$R_n$	W/m <sup>2</sup>	Calculated
● Latent heat flux	$LE$	W/m <sup>2</sup>	Calculated
<b>Inside the PFM</b>			
● Air temperature inside PFM	$T_{in}$	°C	Measured
● Relative humidity inside PFM	$RH_{in}$	%	Measured
● Facial skin temperature	$T_{fsk}$	°C	Measured
● Facial skin wettedness	$w$	–	Measured
● Convection via facial skin	$C_{fsk}$	W/m <sup>2</sup>	Calculated
● Evaporation via facial skin	$E_{fsk}$	W/m <sup>2</sup>	Calculated
● Radiation via facial skin	$R_{fsk}$	W/m <sup>2</sup>	Calculated
● Convection via respiration	$C_{res}$	W/m <sup>2</sup>	Calculated
● Evaporation via respiration	$E_{res}$	W/m <sup>2</sup>	Calculated
● Conduction from PFM surface	$G_{pfm}$	W/m <sup>2</sup>	Calculated
● Heat loss from leakage	$Q$	W/m <sup>2</sup>	Calculated
● Heat flux from facial skin	$H_{fsk}$	W/m <sup>2</sup>	Measured
<b>PFM parameters</b>			
● Albedo of PFM surface	$a_{pfm}$	%	Measured
● Dead space volume	$V_{pfm}$	m <sup>3</sup>	Measured



**Table 2**  
Inputs in the HEATS model.

	Symbol	Unit
<b>Meteorological parameters</b>		
● Air temperature	$T_a$	°C
● Wind speed	$v'$	m/s
● Air vapor pressure	$e$	hPa
● Relative humidity	$RH_a$	%
● Air pressure	$p$	hPa
● Ground surface temperature	$T_g$	°C
● Direct solar radiation	$K_{dir}$	W/m <sup>2</sup>
● Diffuse solar radiation	$K_{dif}$	W/m <sup>2</sup>
● Reflected solar radiation	$K_{ref}$	W/m <sup>2</sup>
● Longwave radiation from air	$L_a$	W/m <sup>2</sup>
● Longwave radiation from ground	$L_g$	W/m <sup>2</sup>
● Cloudiness	$N$	%
● Sun altitude	$hSl$	°
<b>Terrain data</b>		
● Gradient data	$slope$	°
<b>Physiological parameters</b>		
● Metabolic heat production	$M$	W/m <sup>2</sup>
● Skin temperature	$T_s$	°C
● Motion velocity	$v$	m/s
<b>PFM parameters</b>		
● Albedo of PFM surface	$a_{pfm}$	%
● Dead space volume	$V_{pfm}$	m <sup>3</sup>
<b>Clothing properties</b>		
● Albedo of clothing	$a$	%
● Clothing insulation	$I_{cl}$	clo

### 2.3. Field experiments and model evaluation


Field experiments were conducted to investigate the impact of different activity levels on the PFM microenvironment and human thermal stress under realistic hot and humid climatic conditions in Hong Kong between July and September 2020. A typical PFM form, i.e., the disposable surgical mask (Table 4), was selected for the following experiments. A total of five male participants were recruited attending college or graduate school in this study. The age, height, weight were 24 years ( $\pm 2$ ), 176 cm ( $\pm 3$ ), 70 kg ( $\pm 5$ ), respectively. The participants were briefed on the purpose, design, and experimental procedures of the study, and an informed consent was documented. To standardize the thermal burden from clothing other than the respirators, all participants were required to test with similar clothes with 0.4 clo clothing insulation according to ANSI/ASHRAE Standard 55–2017 [39], including a white T-shirt (100% cotton), shorts (65% polyester and 35% rayon), ankle (100% cotton), and sports shoes. The study was approved by the Human Research Ethics Committee, The University of Hong Kong (EA200158).

Each participant was tested in six scenarios (unshaded), including (a) standing still for 50 min, (b) walking on a flat terrain (0°) for 50 min, and (c) climbing on 30° sloped stairs for 50 min, either wearing a PFM or without wearing a PFM. During each experiment, (a) meteorological variables including  $T_a$ ,  $RH_a$ ,  $v'$ , and  $R_n$ , (b) skin-based thermo-physiological variables including  $T_{fsk}$ ,  $w$ , TEWL, and  $H_{fsk}$ , and (c) PFM micro-environmental variables including  $T_{in}$ ,  $RH_{in}$ ,  $O_2$ , and  $CO_2$  were measured simultaneously (Table 1). The duration of each experiment is 50 min with the first 20 min as the acclimatization period and the latter 30 min as the steady period (Fig. 2). During the experiments, there were two sets of equipment, including (1) small portable devices such as iButtons, heat flux sensors,  $CO_2/O_2$  sensors, for continuously measuring air temperature & humidity ( $T_{in}$ ,  $RH_{in}$ ), heat flux ( $H_{fsk}$ ),  $CO_2$  and  $O_2$  inside the facemask, respectively, and (2) large non-portable devices including the weather station for continuously measuring meteorological information, as well as the infrared camera and DermaLab Combo for discretely recording the thermal infrared images and skin conditions ( $w$ , TEWL) in the facial area, respectively. The measurement equipment used in these experiments is depicted in Table 3. In particular, Fig. 3 shows the detailed measurement set-up in the facial area. Fig. 3a shows six measurement sites of skin-based thermo-physiological variables on the facial

**Table 3**  
Meteorological and thermo-physiological quantities measured and instruments.

Parameters	Instrument	Specifications
<b>Meteorological measurements</b>		
● Air temperature	MaxiMet GMX 541 compact weather station (Gill Instruments, UK)	Range: −40–70 °C Accuracy: $\pm 0.3$ °C
● Relative humidity		Range: 0%–100% Accuracy: $\pm 2\%$
● Wind speed		Range: 0.1–60 m/s Accuracy: $\pm 3\%$
● Solar radiation		Range: 0–1,600 W/m <sup>2</sup> Accuracy: $\pm 1$ W/m <sup>2</sup>
<b>Skin-based thermo-physiological quantity</b>		
● Skin temperature	Dermal combo probes (Cortex Technology, Denmark) A310 Infrared thermographic camera (FLIR®, USA)	Range: 0–50 °C Accuracy: $\pm 0.1$ °C Range: 20–350 °C Accuracy: $\pm 0.1$ °C
● Hydration	Conductance (single frequency) electrode in flat-faced probe (Cortex DermaLab® System, Denmark)	Range: 0–9,999 $\mu$ S Accuracy: $\pm 5\%$
● TEWL	Vapor diffusion gradient probe (Cortex DermaLab® System, Denmark)	Range: 0–250 g/m <sup>2</sup> /h Accuracy: $\pm 5\%$
● Heat flux	PHFS-01 heat flux sensors (FluxTeq, USA)	Range: $\pm 150$ kW/m <sup>2</sup> Accuracy: $\pm 5\%$
<b>Microclimate inside the PFM</b>		
● Air temperature	Maxim-integrated iButtons (Digi-Key Electronics, USA)	Range: 40–85 °C Accuracy: $\pm 0.1$ °C
● Relative humidity		Range: 0–100% Accuracy: $\pm 2.5\%$
● $CO_2$	K33 ELG 10,000 ppm $CO_2$ sensor (CO2METER, USA)	Range: 10,000 ppm Accuracy: $\pm 3\%$
● $O_2$	UV Flux Oxygen Smart Sensor (CO2METER, USA)	Range: 0–25% Accuracy: $\pm 2\%$

**Table 4**  
Specific features of PFMs used in this study.

Property	Specifications
Appearance	
Classification Standard	Medical surgical masks YY0469-2011
Inner dimensions (length × width)	17.0 cm × 9.0 cm
Materials/Usage	25 g/m <sup>2</sup> high standard filter layer + 2 nonwovens/ Disposable
Filter classification	BFE > 95%, PFE > 70%
Size/Weight	Standard/3.0 g
Exhalation valve	No
Pressure difference	35.5 Pa/cm <sup>2</sup>
Albedo	24%
Dead space volume	90–180 mL

area, including sites 1–4 inside the PFM and sites 5–6 outside the PFM. In addition, Fig. 3b shows the set-up of two sensors including an iButton sensor and a gas analyser for measuring ( $T_{in}$ ,  $RH_{in}$ ) and ( $O_2$ ,  $CO_2$ ), respectively, in the PFM microenvironment. The iButton sensor was fixed on the inner surface of PFM pointing inward with a 0.5-cm distance from the mouth. The gas analyser was connected with a tube positioned inside the PFM so that the air in the PFM microenvironment can be

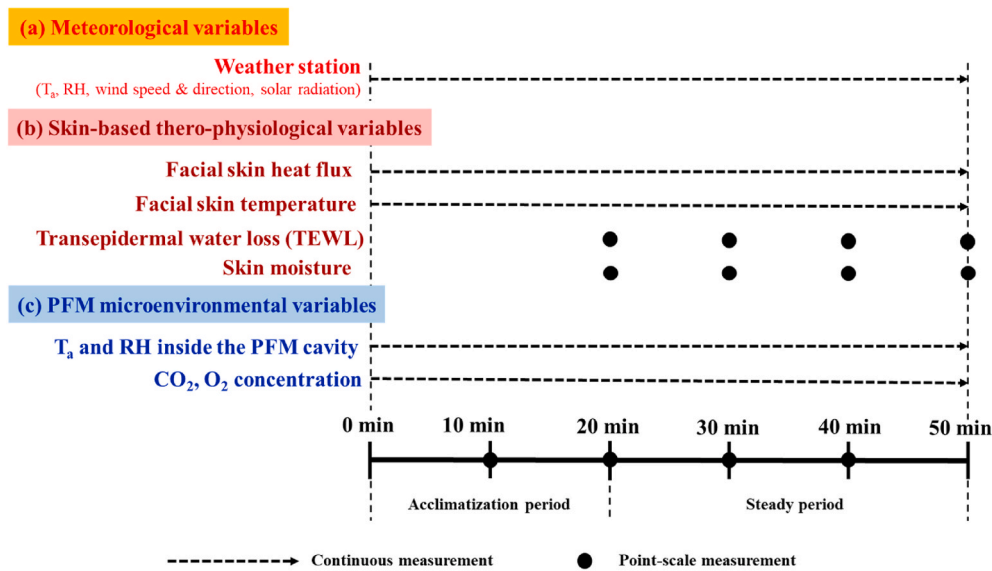


Fig. 2. Measurement schedules of skin-based thermo-physiology and microclimate inside the PFMs during exercising in hot-and-humid outdoor environment (the first 20 min is the acclimatization period; the latter 30 min is the steady period).

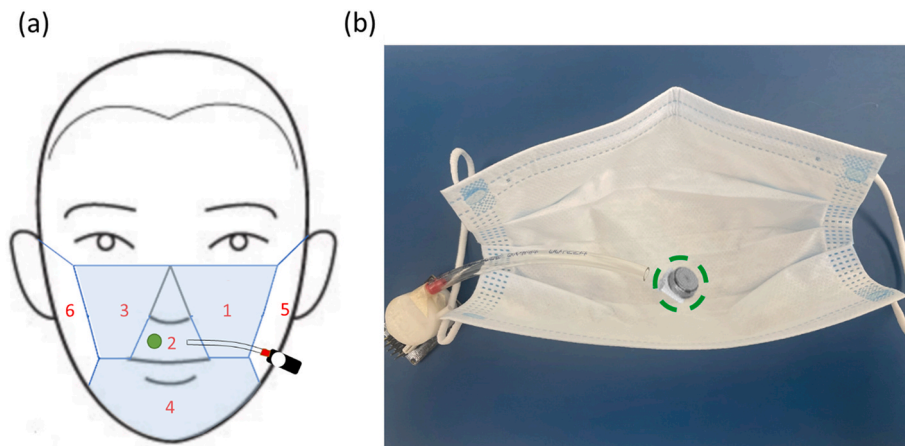


Fig. 3. Sites of measurement for (a) the thermo-physiological parameters inside the PFM (sites 1–4) and outside the mask (sites 5–6), and (b) locations of the iButton sensor (green circle) and the gas analyser (black box). (For interpretation of the references to colour in this figure legend, the reader is referred to the Web version of this article.)

withdrawn and analysed (Fig. 3a). Experimental results can be used for model validation and will be elaborated in section 3.1.

### 2.4. Model simulation scenarios

After model validation, this newly developed HEATS model framework will be applied to simulate the spatiotemporal variations of human thermal stress with and without PFMs over Hong Kong during a typical heat wave event (22–27 June 2016). To drive the model, spatial terrain slope map (30 m × 30 m) (Fig. 4a) and meteorological data at 15 typical meteorological stations (6 rural stations and 9 urban stations) (Fig. 4b) were collected from CEDD [41] and HKO [42], respectively. Significant spatial heterogeneity of terrain slopes and meteorological conditions (e.g., air temperature and absolute humidity) in urban and rural areas can be seen in Fig. 4c and 4d, respectively. First, to investigate the differences of PFM-aggravated human thermal stresses between urban and rural areas due to heterogeneous terrain slopes and meteorological conditions, we conducted a sensitivity test of PST by (1) changing terrain slopes from 0° to 60°, (2) changing meteorological input (urban/rural), and (3) changing PFM wearing status (with/without). Second, to

investigate the spatial variation of PFM-aggravated human thermal stress over Hong Kong, we selected the most uncomfortable period (1:00 p.m., 26 June 2016) and derived the spatial PST maps with and without PFM via the HEATS model. Detailed results can be seen in section 3.2 and 3.3.

## 3. Results

### 3.1. PFM experimental results and model validation

In this section, we analysed the experimental results of facial thermal conditions due to PFMs under three different activity levels (standing, walking, and climbing) as described in section 2.2. First, the use of PFM led to significant increases in the facial skin temperature (up to 2.6 °C) (Fig. 5) and moisture (105.8%–531.7%) under different activity levels (Fig. 5c). Besides, a hot-humid PFM microenvironment can be seen with  $T_a$  and  $RH$  increments of 3.0 °C and 10%~20% respectively, compared to ambient air (Fig. 8a and Fig. 8a). Furthermore, the PFM microenvironment was significantly aggravated by increasing activity levels (standing-walking-climbing), with  $T_a$  increasing from 34.3 °C to 35 °C

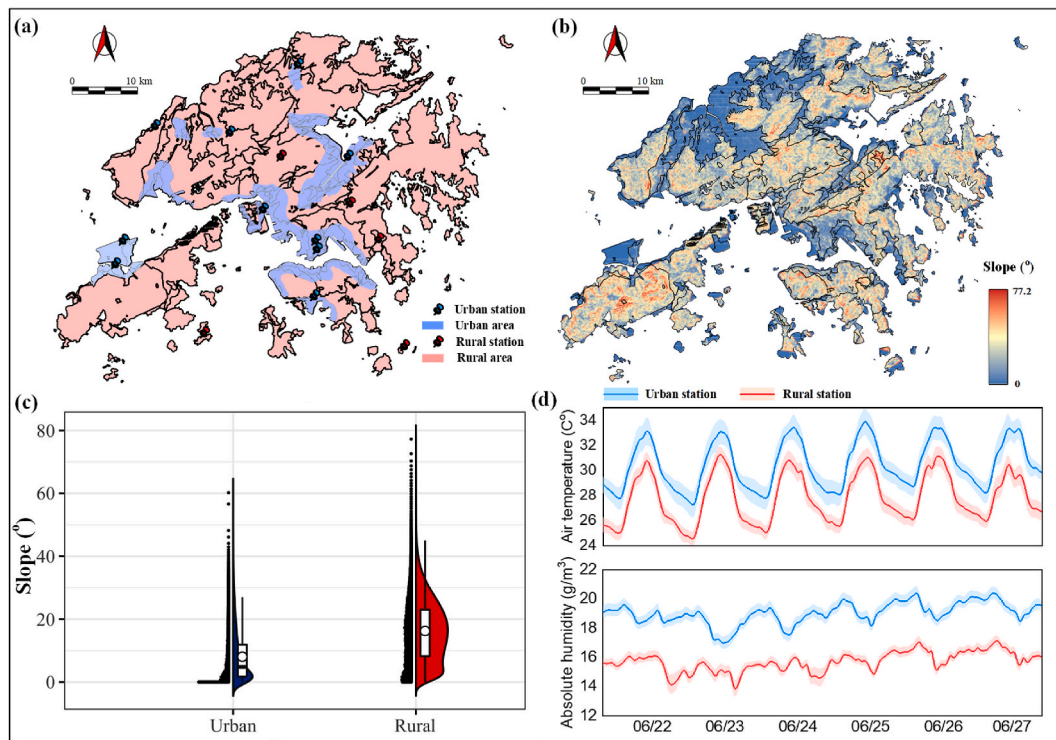


Fig. 4. Demonstration of (a) slope data of Hong Kong, (b) meteorological data, (c) slope ranges in urban and rural areas, (d) average air temperature and absolute humidity in urban and rural areas.

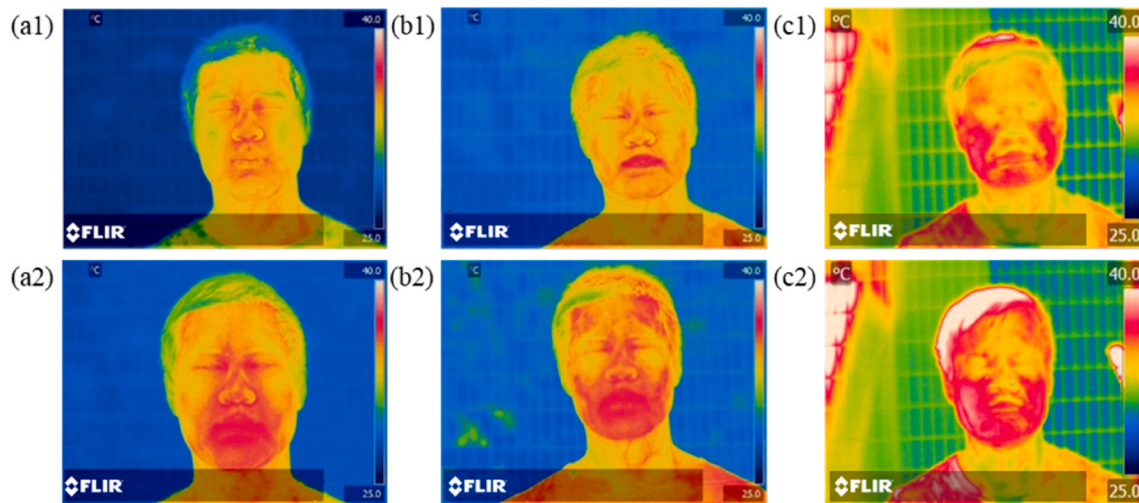


Fig. 5. Thermal infrared images of the subject when (a) standing, (b) walking, and (c) climbing at 30° (1-without PFM, 2-with PFM) under solid solar radiation after 30 min.

(Fig. 8a), and RH increasing from 82% to 91% (Fig. 8b). High temperature and high humidity will further restrain heat convection and sweat evaporation by increasing the facial skin hydration (up to 400%) (Fig. 8c) and reducing the facial TEWL (up to 30 g/m<sup>2</sup>-h) (Fig. 8d). Besides, detailed measured data about the PFM-induced facial thermal stress can be found in Table 5. The suppressed heat dissipation from facial skin and respiration due to PFMs can modify the human energy balance and contribute to an elevated PFM-induced heat load ( $S_{PFM}$ ). On the other hand, measurements of facial skin temperature,  $T_a$  and RH of the PFM cavity, and local meteorological parameters were used to drive the proposed PFM-inclusive HEATS model and to derive facial heat fluxes ( $S_{PFM}$ ) under the three different activity scenarios, which were then compared against measurements (Fig. 6e). From Fig. 6e, we can see

that the model can capture the temporal variation of  $S_{PFM}$  with reasonable accuracy and  $S_{PFM}$  increased dramatically from 50 to 500 W/m<sup>2</sup> with increasing activity intensities and time durations.

### 3.2. Temporal variation of PFM-inclusive thermal stress in urban and rural areas

To investigate the differences of PFM-aggravated thermal stresses in urban and rural areas, we conducted sensitivity analysis for the HEATS model and compared simulated PST values under 28 scenarios (Fig. 7) following the input recipes described in section 2.3. First, since Hong Kong is featured with heterogeneous landscapes with terrain slopes ranging from 0° to 77° (Fig. 4c), different terrain slopes can lead to



**Table 5**  
Detailed measured data about the PFM-induced facial thermal stress.

PFM-related variables	With PFM			Without PFM			Difference		
	Min	Max	Mean	Min	Max	Mean	$\Delta$ Min	$\Delta$ Max	$\Delta$ Mean
<b>Facial skin temperature (°C)</b>									
● Standing still	35.4	37.1	36.3	33.7	35.7	34.7	1.4	1.7	1.6
● Walking on flat terrains	35.7	37.5	36.6	33.8	36.2	35.0	1.3	1.9	1.6
● Walking on 30° stairs	36.7	38.6	37.5	34.9	36.7	35.8	1.8	2.6	2.2
<b>Skin moisture (<math>\mu</math>S)</b>									
● Standing still	1023	1371	1197	829	1173	1069	194	198	128
● Walking on flat terrains	2187	2882	2535	980	1607	1167	1207	1275	1368
● Walking on 30° stairs	3371	4207	3790	1899	2186	2042	1472	2021	1748
<b>TEWL (<math>\text{gm}^{-2}\text{h}^{-1}</math>)</b>									
● Standing still	14.8	19.1	17.1	20.5	27.1	23.5	-3.7	-9.7	-6.4
● Walking on flat terrains	16.6	24.9	21.1	31.5	41.2	35.0	-7.7	-16.3	-13.9
● Walking on 30° stairs	25.3	35.7	30.2	55.5	61.4	59.0	-25.7	-30.5	-28.8
<b>Air temperature inside PFM (°C)</b>									
● Standing still	34.1	35.1	34.3	31.7	32.6	32.2	2.4	2.5	2.1
● Walking on flat terrains	34.6	35.6	34.9	32.0	33.8	32.9	1.8	2.6	2.0
● Walking on 30° stairs	33.6	35.6	34.8	31.5	31.7	31.6	2.1	3.9	3.2
<b>Relative humidity inside PFM (%)</b>									
● Standing still	77.6	85.5	81.6	70.0	72.0	71.0	7.6	13.5	10.6
● Walking on flat terrains	80.5	86.6	85.1	60.0	68.0	65.0	18.6	20.5	20.1
● Walking on 30° stairs	89.1	95.0	91.2	68.0	70.0	69.0	21.1	25.0	22.2

different PST values due to the variation of exertion and activity levels of residents when walking or climbing. It can be seen from Fig. 8 that with a slope increment of 10°, PST can be increased by 1.3–3.9 °C in both urban and rural areas, implying more heat burden under increased activity intensities. Residents walking on a flat terrain (0°) with PFMs may feel equivalent thermal stress as walking on an 30° inclined terrain without PFMs. On the other hand, it is noteworthy that urban terrain slope significantly varies from 0° to 60° in the Hong Kong metropolitan area (Fig. 4c), resulting in that urban residents tend to suffer from aggravated thermal stress with a maximum PST increment of more than 20 °C due to the compound effects of PFM wearing and high-intensity activity levels such as climbing during their daily life (Fig. 7a).

Second, urban area was observed with higher temperature (1.4–2.3 °C) and higher absolute humidity (2.6–4.3 g/m<sup>3</sup>) than rural area during the selected heat wave event (Fig. 4d), owing to the urban heat island (UHI) and urban moisture island (UMI) effects [23,43]. The synergistic UHI and UMI effects may further constrain the heat dissipation of human body via thermal radiation/convection and sweat evaporation, respectively, leading to aggravated thermal stress. Particularly, severer PFM-inclusive human thermal stress has been identified in urban areas than in rural areas at night, possibly owing to nocturnal UHI and UMI, which are attributed to longwave radiation from massive-engineered surfaces, inhibited condensation due to high temperature, as well as anthropogenic heat and moisture sources [44–47]. For example, residents walking on the inclined terrain with a slope of 20° will feel ‘hot’ (Level-2 stress) in urban areas while feeling ‘warm’ (Level 1-stress) in rural areas at night (Fig. 7). If wearing PFMs, the daytime maximum PST of residents can be increased from 57 °C to 64 °C in urban areas and from 55 °C to 62 °C in rural areas, while the night-time maximum PST can be increased from 27 °C to 37 °C in urban areas and from 25 °C to 35 °C in rural areas. This offers a caveat for urban residents that there are significantly higher heat risks when doing outdoor activities with PFMs during the pandemic at both daytime and night-time, night-time heat risks cannot be overlooked.

### 3.3. Spatial variation of PFM-inclusive thermal stress at the hottest period

To investigate PFM aggravated heat risks over the whole Hong Kong metropolitan area, we derived the spatial map of PST without and with PFM via the HEATS model for the hottest period (specifically, 1:00 p.m. 26 Jun 2016) during the selected heat wave event (Fig. 9). The spatial variation of PST values over Hong Kong are 37.3–54.8 °C without PFM (Figs. 9a) and 38.7–58.7 °C with PFM (Fig. 9b). By comparing Fig. 9a

and b, it is evident that the use of PFM contributes to an average PST increment of 5.0 °C, which leads to an additional percentage of ‘sweltering’ (Level-4 stress with highest heat risks) by 158.4% over Hong Kong, especially in rugged hills when people are hiking.

Hong Kong has 24 country parks comprising more than 400 hiking trails, frequented by 10 million visitors every year. With many restaurants, beaches, and gyms closed during the pandemic, a near 100–150% increase in the number of hikers was found in the first half of 2020 compared to 2019 [48]. As a result, hikers are facing a tough dilemma that wearing PFM will suffer from intensive thermal stress, while ditching PFMs will increase the infection risk.

To investigate the impact of PFM on the thermal stress of hikers over different hiking trails, we select three hiking trails with the same traveling distance (10 km) but different difficulty levels according to Shenandoah Hiking Difficulty protocol [49], including Wu Kau Tang trail (level 1 with an average slope of 11°), Dragon Backtrail (level 3 with an average slope of 17°), and Tsing Shan Monastery trail (level 5 with an average slope of 43°). Fig. 10 indicates that human thermal stress can be aggravated due to the wearing of PFM and the increase of difficulty levels of hiking trails. During the hottest period, the average PST values of hikers in the level 1, 3, and 5 trails are 44.4 °C, 46.5 °C, and 48.0 °C, respectively, without PFMs, and can be increased to 46.2 °C, 49.2 °C, and 52.5 °C, respectively with PFMs. In addition, the usage of PFMs can lead to increased heat risks in all hiking trails, for example, the probability of ‘very hot’ risks will be increased from 40.3% to 52.1% in the Level-1 trail, from 65.0% to 85.1% in the Level-2 trail, and from 80.0% to 88.8% in the Level-3 trail.

## 4. Discussion

### 4.1. Breathing comfort of PFMs

Extreme heat events add extra heat risks for residents in PFM-wearing culture. Many cases of the PFM-related heat stroke or even death was reported in 2020, which causes widespread concern about the side effects of PFMs. During high-intensity activities like hiking, human bodies need to consume more oxygen with accelerated or doubled breathing rates. Since PFMs are not well ventilated and close to the face, they may quickly get damp due to intensive breathing and sweating. Significant CO<sub>2</sub> surges and O<sub>2</sub> reductions were found inside sweaty PFM during our field experiment (Fig. 11), implying that sweaty PFMs can aggravate the breathing discomfort sensation. Although wearing PFMs is uncomfortable in breathing sensation and thermal sensation, it is

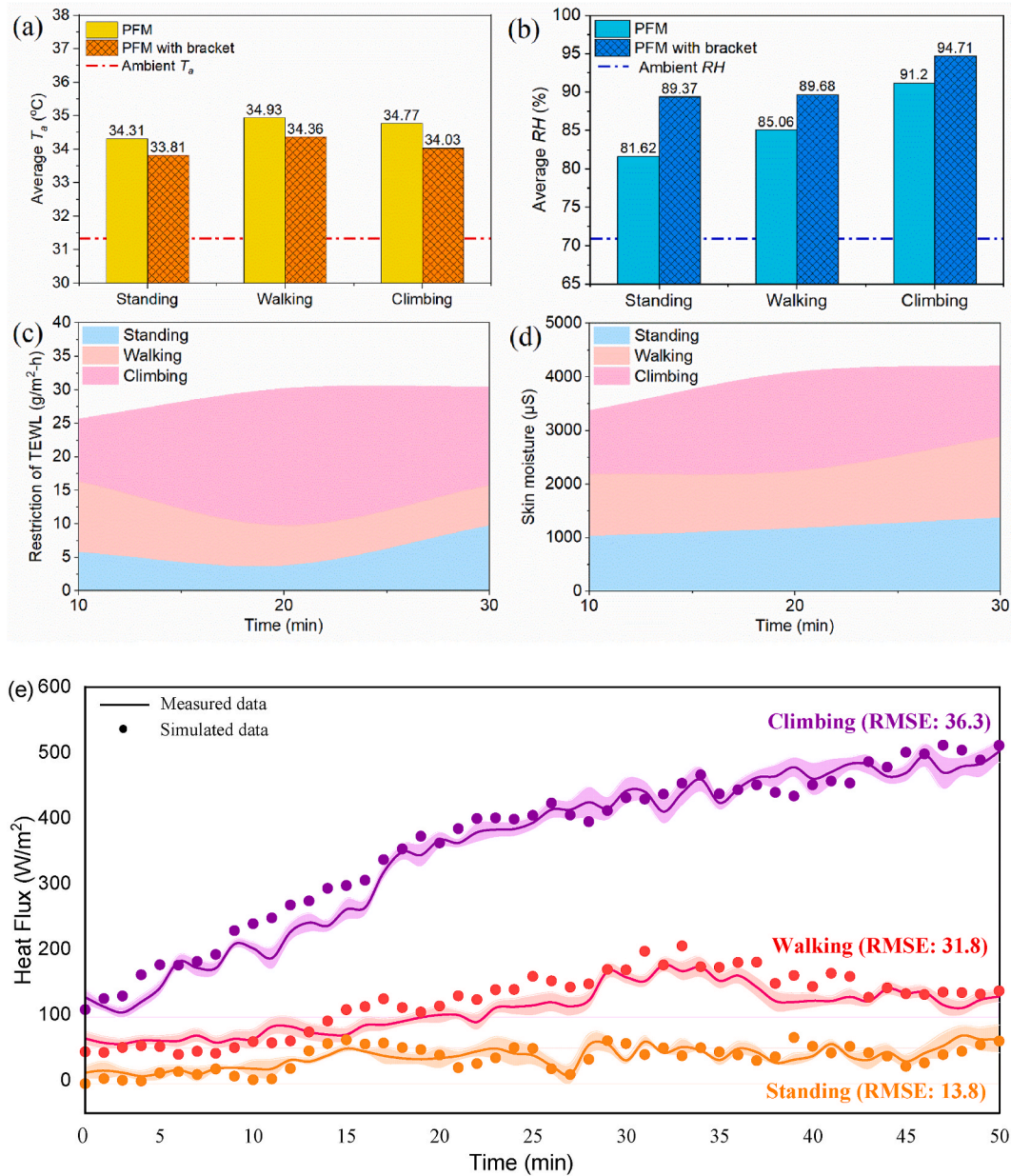


Fig. 6. Measurement of (a) air temperature ( $T_a$ ), (b) relative humidity (RH), (c) restriction of facial skin sweating rate, (d) skin moisture, (e) validation of facial skin heat flux.

unavoidable as a necessary personal protective equipment during the pandemic. To deal with the dilemma, hikers sometimes use mask brackets to improve their breathing and thermal comfort, since mask brackets can help keep a constant-volume microenvironment for heat and air exchanges. With the use of mask bracket, we found a decrease in  $T_a$  but an increase in RH inside the cavity (Fig. 6a and b), possibly due to enhanced sweat evaporative cooling. However, the accumulated moisture inside the cavity may lead to another possibility of heatstroke due to a reduced hydration level since the damp PFM microenvironment tends to make people feel fewer signs of thirst [50].

#### 4.2. Implications on public health and policymaking

The COVID-19 pandemic has amplified health risks in hot seasons for people worldwide, especially for the following groups who are vulnerable to both infection risk and heat stress risk, including people with underlying conditions (respiratory, cardiovascular and cerebrovascular

diseases as well as mental health issues), the elderly, children, pregnant women, outdoor workers, athletes, health workers, the economically disadvantaged who might lack of essential cooling and hygiene facilities, and those who have been first infected and then discharged from hospitals after treatment with COVID-19 [1,5,41]. During the pandemic, the use of PFMs in hot seasons can lead to more hospitalization rates of heatstroke due to an aggravated level of thermal stress and a reduced level of hydration since the damp and humid PFM microenvironment tends to make people feel less signs of thirst, according to a report “Wearing masks in summer can lead to heatstroke; Japan doctors urge self-hydration” from the Japan National Daily News [50]. Therefore, it is of great importance for the government and public to be better prepared for the dual challenges of infection risk and heat risk. For example, the Centers for Disease Control and Prevention (CDC) in the US published a document “Employer information for heat stress prevention during the COVID-19 Pandemic” on 26 Aug 2020 [52], which provides heat illness prevention guidelines for employers to better protect outdoor workers



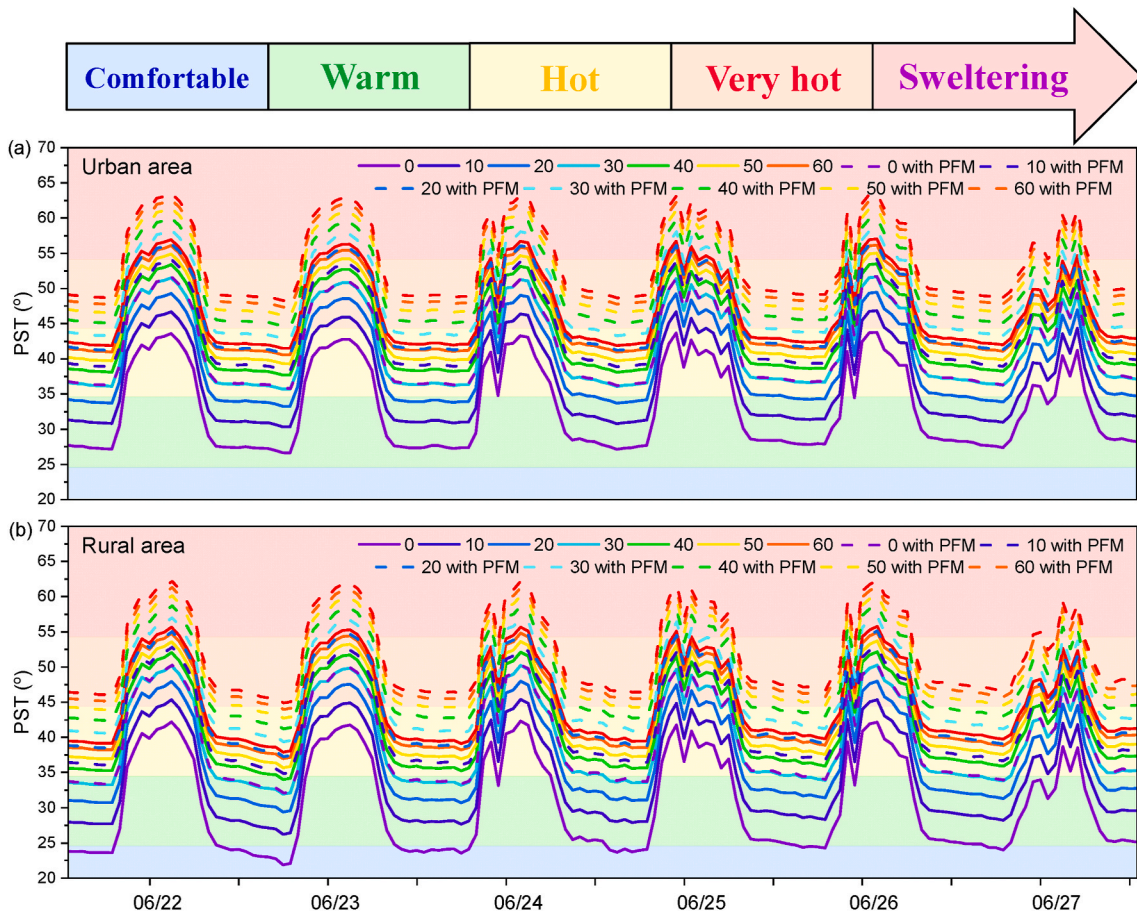


Fig. 7. PST with and without PFM of (a) urban area, (b) rural area per 10° interval between 0° and 60°.

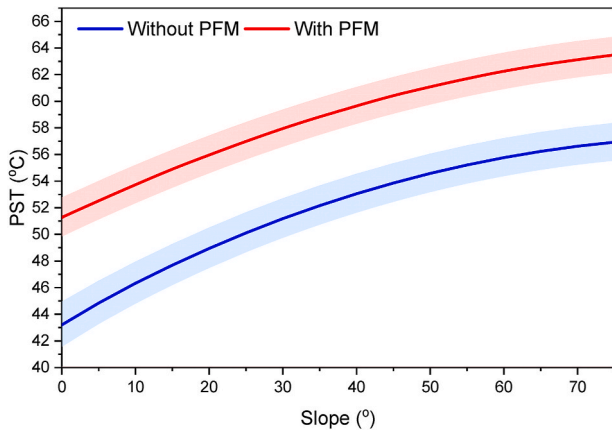


Fig. 8. Variation of PST with slope increment from 0° to 75° to cover the terrain gradient range in Hong Kong.

from the dual risks of the pandemic and heat stress.

In this study, we predicted a fine-resolution PFM-inclusive thermal stress and heat warning map covering Hong Kong, which can offer significant guidance for the public and the government. For example, the government may build more cooling and rehydration infrastructure in the neighbourhoods that prone to PFM-inclusive heat stress. Urban Renewal Authority (URA) can boost more air-conditioned bus depots [55] in the main public transport interchanges. More pavilions, pergolas and gazebos with hydration stations can be built along the hiking trails to protect the hikers from heat-related risks such as thermoplegia and

dehydration. Besides, an early warning system needs to be established via the cross-departmental coordination between Hong Kong Observatory (HKO), Information Service Department (ISD), Centre for Health Protection of Department of Health (CHPDH), and Interactive Employment Service of Labor Department (IESLD). The system can provide heat illness prevention guidelines for employers to better protect outdoor workers from the dual risks of the pandemic and heat stress. The procedures may include adjusting work/rest schedules and daily work completion targets during hot weather, providing more cooling and rehydration stations, and making emergency first-aid plans [52]. On the other hand, the public can also benefit from this study, such as planning or altering their outdoor activity schedules according to the PFM-inclusive heat risk forecasts. For example, traffic policemen and building/road construction workers shall be aware of the aggravated thermal stress in their working areas and make good preparations beforehand, pedestrians can choose paths crossing more comfortable neighbourhoods (shaded areas, green/blue spaces, relatively flat paths) with less heat risks, and hikers can make less dangerous plans such as choosing hiking trails with smaller terrain slopes, more tree canopy shade, or more pavilions, using mask frame to improve thermal and breathing comfort, and bringing spare clean masks to replace sweated ones.

### 5. Concluding remarks

In this study, we investigated the aggravated human thermal stress due to PFMs over Hong Kong via both field experiments and model simulations. In the field experimental phase, we conducted detailed observations on facial thermo-physiological responses and the micro-environment within the PFM cavity. It was found that large amounts of

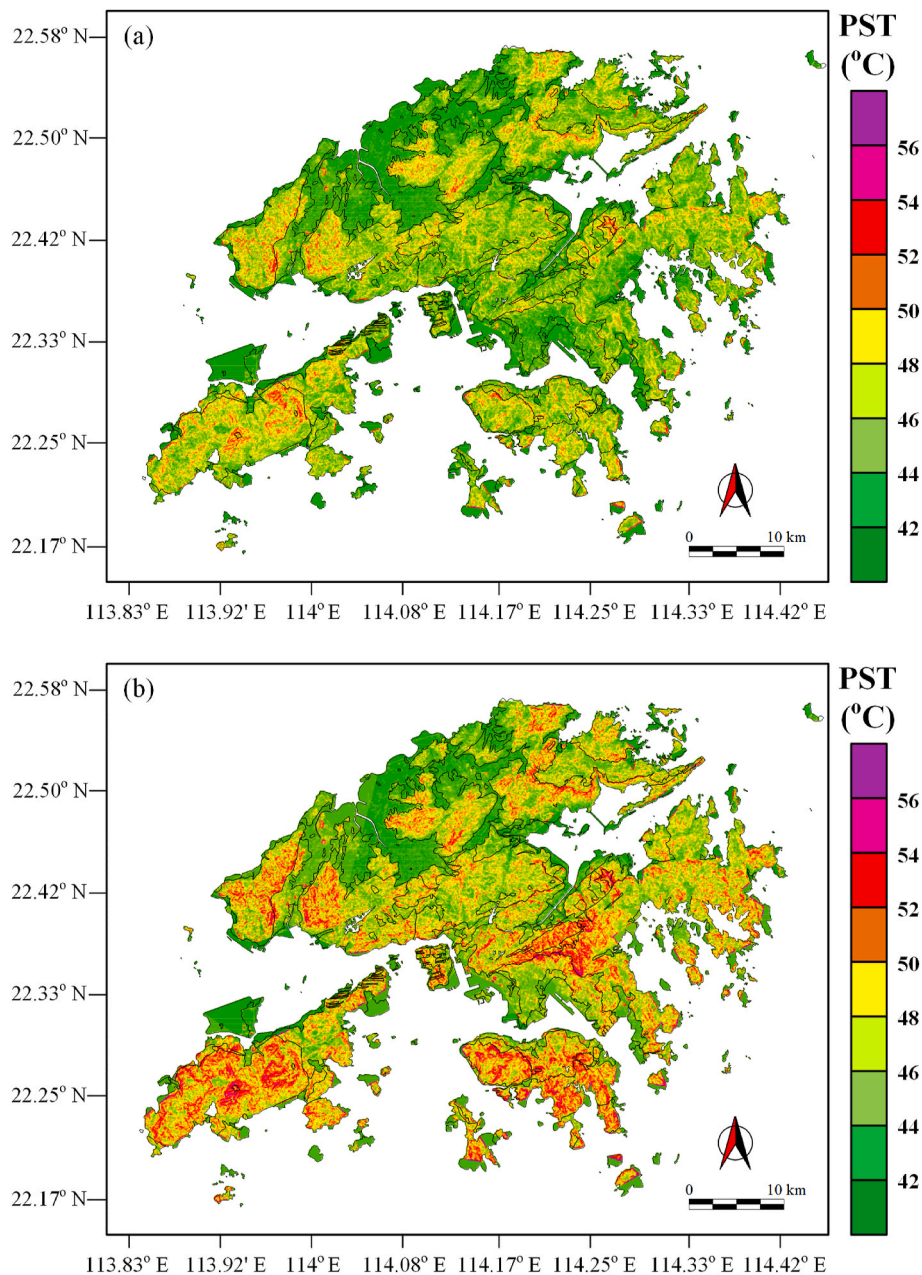


**Fig. 9.** Simulated PST of Top-HEATS over Hong Kong at 1:00 p.m. 26 Jun 2016 under scenarios (a) without PFM, and (b) with PFM.

facial heat fluxes from skin and respiration ( $50\text{--}500\text{ W/m}^2$ ) can be trapped in the hot and humid PFM cavity ( $T_a$ :  $34\text{--}35\text{ }^\circ\text{C}$ ,  $RH$ :  $80\text{--}95\%$ ) due to restrained heat dissipation, which leads to aggravated facial thermal burden, especially during high-intensity activities. In the model simulation phase, first we developed a new human thermal stress model named HEATS by considering modified human-environment heat exchanges due to PFM wearing under realistic climatic and topographical conditions. This new model was then applied to simulate spatiotemporal variations of PFM-aggravated human thermal stress during a typical heat wave event (22–27 June 2016) over Hong Kong. Our model simulation results showed that the use of PFMs can significantly aggravate human thermal stress over Hong Kong with a PST increment of  $7.0\text{--}8.2\text{ }^\circ\text{C}$  and additional 158.4% neighbourhoods exposing to the severest heat risks (Level 4-sweating). Particularly, urban residents may suffer more intensive PFM-aggravated thermal stress at night than rural residents due to synergistic urban heat and moisture island effects. Besides, PFM-inclusive PST was found to increase nonlinearly with

terrain slopes at a rate of  $1.3\text{--}3.9\text{ }^\circ\text{C}/10^\circ$ , owing to increased metabolic heat production when climbing on inclined terrains, which is usually overlooked but very important for residents in mountainous cities. Residents walking on a flat terrain ( $0^\circ$ ) with PFMs may feel equivalent thermal stress as walking on an  $30^\circ$  inclined terrain without PFMs. In addition, we found that PFMs not only affect people's thermal comfort, but also breathing comfort. Particularly, a high concentration of  $\text{CO}_2$  and a low concentration of  $\text{O}_2$  were found inside sweaty PFMs, which may cause severe hypoxia and possible disorder of vulnerable people's lungs. It is noteworthy that the use of mask bracket can offer a promising thermal stress mitigation strategy for people during high-intensity activities, since mask bracket is useful to keep a constant volume of the PFM microenvironment for heat and air exchanges. Our timely study on PFM-aggravated thermal stress may offer significant implications for the government, the public, as well as mask design companies under the dual challenges of extreme hot weathers and pandemics.



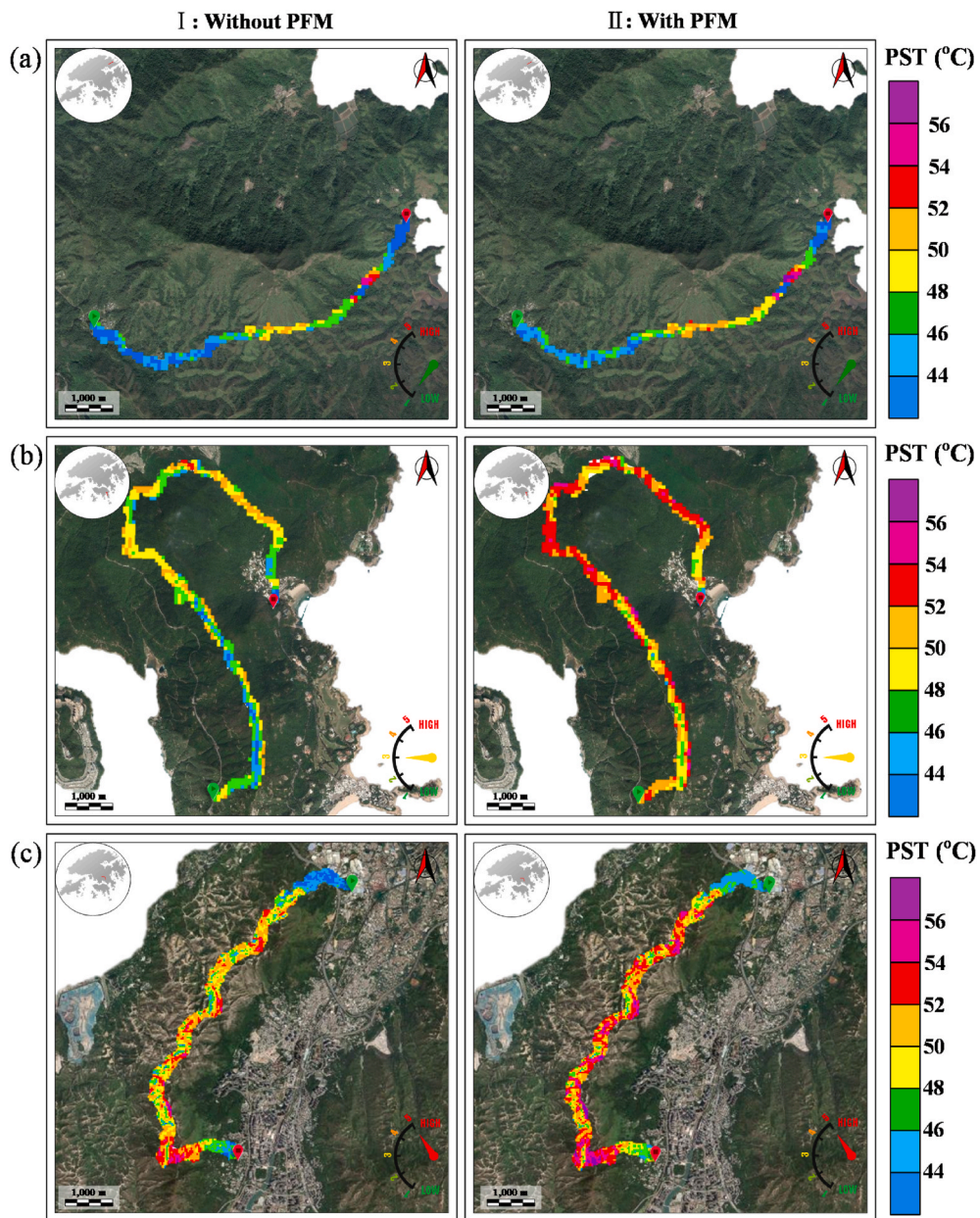


Fig. 10. Human thermal stress variation of (a) Wu Kau Tang (Level 1 trail), (b) Dragon Back (Level 3 trail), and (c) Tsing Shan Monastery (Level 5 trail) with and without PFM.

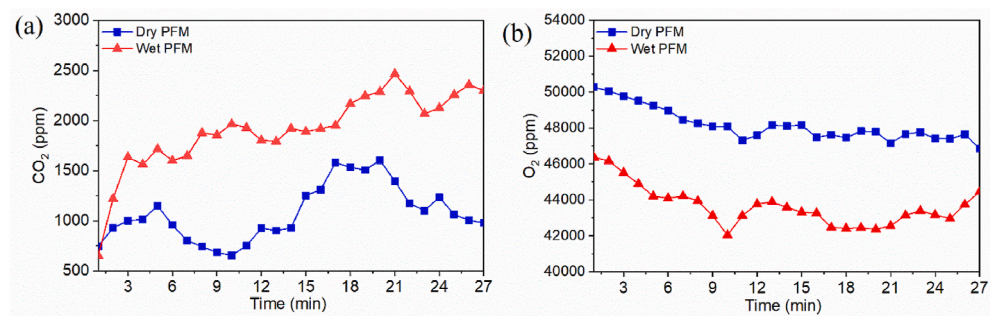


Fig. 11. Measurement of (a) CO<sub>2</sub> and (b) O<sub>2</sub> in the PFM cavity.

## Declaration of competing interest

The authors declare that they have no known competing financial interests or personal relationships that could have appeared to influence the work reported in this paper.

## Acknowledgments

This work is supported by the Hong Kong Research Grants Council

(RGC) General Research Fund (Project number: 17208021) and Hong Kong RGC Early Career Scheme Fund (Project number: 27208220), The University of Hong Kong (HKU) University Research Committee Seed fund for basic research for new staff (Project number: 201909185052), HKU Faculty of Engineering COVID-19 Action Seed Funding, and HKU start-up fund “Climate change prediction and adaptation for energy security and human health”.

## Appendix 1. The calculation of the heat and moisture transfer between human body (except the face) and environment

Heat and moisture transfer between human body (except the face) and environment, i.e., the heat dissipation via convection and evaporation can be calculated by [14,38]:

$$(C + E)_{body} = hc \cdot (T_a - T_s) \cdot Irc + he \cdot (e - es) \cdot w \cdot Ie - [0.42 \cdot (M - 58) - 5.04] \quad (A1-1)$$

where  $hc$  is the coefficient of convective and radiative heat transfer,  $K/(W \cdot m^2)$ ,  $T_a$  is the ambient air temperature,  $^{\circ}C$ ,  $T_s$  is the mean skin temperature,  $^{\circ}C$ ,  $he$  is the coefficient of evaporative heat transfer,  $hPa/(W \cdot m^2)$ ,  $e$  is the air vapor pressure,  $hPa$ ,  $es$  is the saturated vapor pressure at skin temperature,  $hPa$ ,  $w$  is the skin wittedness,  $Ie$  is the reduction coefficient of evaporative heat transfer due to clothing (obtained by Eqns. A1-2 [38]),  $Irc$  is the reduction coefficient of convective and radiative heat transfer due to clothing (obtained by Eqns. A1-3 [29]).

$$Ie = \frac{hc'}{hc' + hc} \quad (A1-2)$$

$$Irc = \frac{hc'}{hc' + hc + 21.55 \times 10^{-8} \cdot T_a^3} \quad (A1-3)$$

where  $hc'$  is the coefficient of heat transfer through clothing,  $K/(W \cdot m^2)$  [14],

$$hc' = \frac{0.53 \cdot (0.013p - 0.04T_a - 0.503)}{Icl \cdot (1 - 0.27 \cdot (v + v')^{0.4})} \quad (A1-4)$$

where  $p$  is the ambient air pressure,  $hPa$ ,  $v'$  is wind speed,  $m/s$ .

## Appendix 2. The derivation of Pandolf's predictive equation

The metabolic costs ( $M$ ) of load carriage over complex terrain for human beings can be computed using the Looney's modified version of Pandolf's predictive equation, which was derived from steady-state exercise protocols and proven to be an accurate predictor of metabolic costs [33,36].

$$M = M_1 + M_2 + M_3 + M_4 = 1.5 \cdot m + 2.0 \cdot (m + l) \cdot (l/m)^2 + \eta \cdot (m + l) \cdot (1.5 \cdot v^2 + 0.35 \cdot v \cdot slope) \quad (A-2)$$

where  $m$  is the average human body weight,  $kg$ ,  $l$  is the carriage load,  $kg$ ,  $\eta$  is terrain coefficient (1.0 for hard surfaces or pavements),  $v$  is the walking speed,  $slope$  is the terrain gradient. The total metabolic cost  $M$  combines 4 sub-components,  $M_1$  is the metabolic cost of standing without load, which is proportional to the body's weight ( $m$ ),  $M_2$  is the metabolic cost of standing with load, which is affected by the total weight of body and load ( $m + l$ ) and is fitted as a function of the load-to-weight ratio squared ( $(l/m)^2$ ),  $M_3$  is the metabolic cost of walking on a flat terrain, which is related to a specific terrain form ( $\eta$ ), and is fitted as a function of the walking speed squared ( $v^2$ ),  $M_4$  is the metabolic cost of climbing on an inclined terrain, which is related to a specific terrain form ( $\eta$ ) and total weight ( $m + l$ ) and is fitted as a linear function of the walking speed ( $v$ ) and terrain gradient ( $slope$ ).

## References

- [1] D.O. Åström, B. Forsberg, J. Rocklöv, Heat wave impact on morbidity and mortality in the elderly population: a review of recent studies, *Maturitas* 69 (2011) 99–105, <https://doi.org/10.1016/j.maturitas.2011.03.008>.
- [2] J.K. Rosenthal, P.L. Kinney, K.B. Metzger, Intra-urban vulnerability to heat-related mortality in New York City, 1997–2006, *Health Place* 30 (2014) 45–60, <https://doi.org/10.1016/j.healthplace.2014.07.014>.
- [3] M. Morabito, A. Messeri, A. Crisci, L. Pratali, M. Bonafede, A. Marinaccio, Heat warning and public and workers' health at the time of COVID-19 pandemic, *Sci. Total Environ.* 738 (2020), 140347, <https://doi.org/10.1016/j.scitotenv.2020.140347>.
- [4] Global Heat Health Information Network (GHHN), Protecting health from hot weather during the COVID-19 pandemic, *Tech. Brief.* (2020). Retrieved from, <http://www.ghhn.org/assets/technical-brief-COVID-and-Heat-final.pdf>.
- [5] Roberge R J, Kim J-H, Coca A 2012a protective facemask impact on human thermoregulation: an Overview. *Ann. Occup. Hyg.*, 56, 102–112. <https://doi.org/10.1093/annhyg/mer069>.
- [6] A.B. DuBois, Z.F. Harb, S.H. Fox, Thermal discomfort of respiratory protective devices, *Am. Ind. Hyg. Assoc. J.* 51 (1990) 550–554, <https://doi.org/10.1080/15298669091370086>.
- [7] I.S. Laird, R. Pack, D. Carr, A survey on the use and non-use of respiratory protective equipment in workplaces in a provincial New Zealand city, *Ann. Occup. Hyg.* 37 (1999) 367–376, <https://doi.org/10.1093/annhyg/37.4.367>.
- [8] R.J. Roberge, J.-H. Kim, S.M. Benson, Absence of consequential changes in physiological, thermal and subjective responses from wearing a surgical mask, *Respir. Physiol. Neurobiol.* 181 (2012) 29–35, <https://doi.org/10.1016/j.resp.2012.01.010>.
- [9] R.J. Roberge, J.-H. Kim, S.M. Benson, N95 filtering facepiece respirator dead space temperature and humidity, *J. Occup. Environ. Hyg.* 9 (2012) 166–171, <https://doi.org/10.1080/15459624.2012.660428>.
- [10] R.J. Roberge, S.M. Benson, J.-H. Kim, Thermal burden of N95 filtering facepiece respirators, *Ann. Occup. Hyg.* 56 (2012) 808–814, <https://doi.org/10.1093/annhyg/mes001>.
- [11] Y.-C. Lin, C.-P. Chen, Thermoregulation and thermal sensation in response to wearing tight-fitting respirators and exercising in hot-and-humid indoor

- environment, *Build. Environ.* 160 (2020), 106158, <https://doi.org/10.1016/j.buildenv.2019.05.036>.
- [12] P.O. Fanger, Thermal comfort, Analysis and applications in environmental engineering, Thermal comfort. Analysis and applications in environmental engineering (1970).
- [13] G. Jendritzky, W. Nübler, A model analysing the urban thermal environment in physiologically significant terms, *Arch. Met. Geoph. Biokl.* 29 (1981) 313–326.
- [14] K. Blazejczyk, New climatological and physiological model of the Human Heat Balance outdoor (MENEX) and its applications in bioclimatological studies in different scales, *Zesz Inst Geogr iPrzestrz Zagospod PAN* 28 (1994) 27–58.
- [15] A. Gagge, J. Stolwijk, Y. Nishi, An effective temperature scale based on a simple model of human physiological regulatory response, *Build. Eng.* 77 (1971) 247–262.
- [16] Kaynakli O, Kilic M 2005 Investigation of indoor thermal comfort under transient conditions, *Build. Environ.*, 40, 165–174, <https://doi.org/10.1016/j.buildenv.2004.05.010>.
- [17] E. Foda, K. Sirén, A new approach using the Pierce two-node model for different body parts, *Int. J. Biometeorol.* 55 (2011) 519–532, <https://doi.org/10.1007/s00484-010-0375-4>.
- [18] D. Fiala, Dynamic Simulation of Human Heat Transfer and Thermal Comfort, Doctoral dissertation, De Montfort University, 1998.
- [19] S.I. Tanabe, K. Kobayashi, J. Nakano, Y. Ozeki, M. Konishi, Evaluation of thermal comfort using combined multi-node thermoregulation (65MN) and radiation models and computational fluid dynamics (CFD), *Energy Build.* 34 (2002) 637–646, [https://doi.org/10.1016/S0378-7788\(02\)00014-2](https://doi.org/10.1016/S0378-7788(02)00014-2).
- [20] C. Huizenga, Z. Hui, E. Arens, A model of human physiology and comfort for assessing complex thermal environments, *Build. Environ.* 36 (2001) 691–699, [https://doi.org/10.1016/S0360-1323\(00\)00061-5](https://doi.org/10.1016/S0360-1323(00)00061-5).
- [21] Q. Zhao, Z. Lian, D. Lai, Thermal Comfort models and their developments: a review, *Energy and Built Environment* 2 (2021) 21–33, <https://doi.org/10.1016/j.enbenv.2020.05.007>.
- [22] Hong Kong Observatory (HKO), Climate of Hong Kong, 2021. <https://www.hko.gov.hk/en/cis/climahk.htm>.
- [23] Z. Wang, J. Song, P.W. Chan, Y. Li, The urban moisture island phenomenon and its mechanisms in a high-rise high-density city, *Int J Climatol* 41 (2020) 150–170, <https://doi.org/10.1002/joc.6672>.
- [24] Y. Epstein, D.S. Moran, Thermal comfort and the heat stress indices, *Ind. Health* 44 (2006) 388–398, <https://doi.org/10.2486/indhealth.44.388>.
- [25] E.D. Coffel, R.M. Horton, A. Sherbinin, Temperature and humidity-based projections of a rapid rise in global heat stress exposure during the 21st century, *Environ. Res. Lett.* 13 (2018), 014001, <https://doi.org/10.1088/1748-9326/aaa00e>.
- [26] Land Utilization in Hong Kong, Planning Department of the Government of the Hong Kong Special Administrative Region, 2019. Retrieved from, [https://www.pland.gov.hk/pland\\_en/info\\_serv/statistic/landu.html](https://www.pland.gov.hk/pland_en/info_serv/statistic/landu.html).
- [27] L.W. Ludlow, P.G. Weyand, Walking economy is predictably determined by speed, grade and gravitational load, *J. Appl. Physiol.* 123 (2017) 1288–1302, <https://doi.org/10.1152/jappphysiol.00504.2017>.
- [28] Parsons 2014 *Human Thermal Environments: the Effects of Hot, Moderate, and Cold Environments on Human Health, Comfort, and Performance*. (FL: CRC Press/Taylor & Francis Group).
- [29] K. Blazejczyk, B. Krawczyk, Bioclimatic Research of the Human Heat Balance, Institute of Geography and Spatial Organization, 1994, p. 66.
- [30] C. Zhang, F. Wang, in: J. Hu, B. Kumar, J. Lu (Eds.), *Comfort Management of Fibrous Materials*, Wiley, New York, 2020, p. 857.
- [31] Heat Islands: when Water Refreshes the City, retrieved from <https://www.planet.veolia.com/en/ilots-de-chaleur-quand-l-eau-rafraichit-la-ville>.
- [32] Shutterstock, retrieved from, <https://www.shutterstock.com/zh/image-vector/businessman-start-walking-stairway-first-step-1202545723>.
- [33] K.B. Pandolf, B. Givoni, R.F. Goldman, Predicting energy expenditure with loads while standing or walking very slowly, *J. Appl. Physiol. Respir. Environ. Exerc. Physiol.* 43 (1977) 577–581, <https://doi.org/10.1152/jappphysiol.1977.43.4.577>.
- [34] I.J. Irmischer, K.C. Clarke, Measuring and modeling the speed of human navigation, *Cartogr. Geogr. Inf. Sci.* 45 (2018) 177–186, <https://doi.org/10.1080/15230406.2017.1292150>.
- [35] BS EN ISO 8996 2004 Ergonomics of the Thermal Environment – Determination of Metabolic Rate, pp 34.
- [36] D.P. Looney, W.R. Santee, A.J. Karis, L.A. Blanchard, M.N. Rome, A.J. Carter, A. W. Potter, Metabolic costs of military load carriage over complex terrain, *Mil. Med.* 183 (2018) 357–362, <https://doi.org/10.1093/milmed/usx099>.
- [37] K. Blazejczyk, Influence of Solar Radiation on Skin Temperature in Standing and Walking Subjects Outdoors, in: J.A. Hodgdon, J.H. Heaney, M.J. Buono (Eds.), *Proceedings of the 8th International Conference on Environmental Ergonomics, Environmental ergo-nomics VIII*, San Diego, 1998, pp. 57–60.
- [38] K. Blazejczyk, New Indices to Assess Thermal Risks Outdoors, in: I. Holmér, K. Kuklane, C. Gao (Eds.), *Environmental Ergonomics XI, Proc. Of the 11th International Conference*, 22–26 May, 2005, 2005, pp. 222–225. Ystat, Sweden.
- [39] American National Standards Institute (ANSI), American Society of Heating, Refrigerating and Air-Conditioning Engineers, Inc. (ASHRAE), *Thermal Environmental Conditions for Human Occupancy*, ANSI/ASHRAE Standard 55-2017, ANSI/ASHRAE, Atlanta, GA, 2017.
- [41] Civil Engineering and Development Department (CEDD), Slope of Hong Kong, 2017. <https://opendata.esrichina.hk/datasets/39d3140fa18e4dcaa3d706a6dee7d7b1>.
- [42] Hong Kong Observatory (HKO), Summary of Meteorological and Tidal Observations in Hong Kong, 2019.
- [43] Y. Wang, Y. Li, D.S. Sabatino, A. Martilli, P.W. Chan, Effects of anthropogenic heat due to air-conditioning systems on an extreme high temperature event in Hong Kong, *Environ. Res. Lett.* 13 (2018), 034015, <https://doi.org/10.1088/1748-9326/aaa848>.
- [44] K. Richards, Urban and rural dewfall, surface moisture, and associated canopy-level air temperature and humidity measurements for Vancouver, Canada, *Boundary-Layer Meteorol.* 114 (2005) 143–163, <https://doi.org/10.1007/s10546-004-8947-7>.
- [45] W. Kuttler, S. Weber, J. Schonnefeld, A. Hesselschwerdt, Urban/rural atmospheric water vapour pressure differences and urban moisture excess in Krefeld, Germany, *Int. J. Climatol.* 27 (2007) 2005–2015, <https://doi.org/10.1002/joc.1558>.
- [46] J. Song, Z.-H. Wang, Diurnal changes in urban boundary layer environment induced by urban greening, *Environ. Res. Lett.* 11 (2016), 114018, <https://doi.org/10.1088/1748-9326/11/11/114018>.
- [47] J. Song, Z.-H. Wang, S.W. Myint, C. Wang, The hysteresis effect on surface-air temperature relationship and its implications to urban planning: an examination in Phoenix, Arizona, USA, *Landsc. Urban Plann.* 167 (2017) 198–211, <https://doi.org/10.1016/j.landurbplan.2017.06.024>.
- [48] J. Griffiths, Maintaining Hong Kong's 400 Miles of Hiking Trails, One Step at a Time, 2020. Retrieved from, <https://edition.cnn.com/travel/article/hong-kong-hiking-trails-intl-hnk/index.html>.
- [49] R.M. Wilson, Alaska Hike Search: Designing a Mapping Application for Alaskan Trails and User Contributed Hazards, *PhD Thesis* University of Southern California, Los Angeles, 2020.
- [50] Japan National Daily News (JNDN), Wearing Masks in Summer Can Lead to Heatstroke; Japan Doctors Urge Self-Hydration, 2020 retrieved from, <https://mainichi.jp/english/articles/20200519/p2a/00m/0na/016000c>.
- [52] Centers for Disease Control and Prevention (CDC), What Workers Need to Know about Heat Stress Prevention during the COVID-19 Pandemic, 2020. Retrieved from, <https://www.cdc.gov/coronavirus/2019-ncov/community/organizations/heat-stress-employees.html>.
- [55] Y. Rachel, Hong Kong's Largest Public Transport Interchange, with City's First Air-Conditioned Bus Depots, to Open at Kwun Tong on April 2, 2021. Retrieved from, <https://amp.scmp.com/news/hong-kong/transport/article/3126340/hong-kongs-largest-public-transport-interchange-open-kwun>.